Nonuniform Compressive Strain in Horizontally Aligned Single-Walled Carbon Nanotubes Grown on Single Crystal Quartz

Taner Ozel,[†] Daner Abdula,[‡] Eric Hwang,[‡] and Moonsub Shim[‡,*]

[†]Departments of Physics and [‡]Materials Science and Engineering, University of Illinois at Urbana−Champaign, Urbana, Illinois 61801

ABSTRACT Interactions with the substrate that allow near perfect horizontal alignment in combination with large difference in the coefficient of thermal expansion are shown to lead to uniaxial compressive strain in as-grown single-walled carbon nanotubes on single crystal quartz. Temperature dependence of Raman G-band spectra along the length of individual nanotubes reveals that the compressive strain is nonuniform and can be larger than 1% locally at room temperature. A response of 27 cm^{-1} upshift per % compressive strain is estimated for the G-band longitudinal optical phonon mode of semiconducting nanotubes. Comparison of Raman and atomic force microscope images suggests that the nonuniformity of the compression arises from the surface roughness induced by polishing. Effects of device fabrication steps on the nonuniform strain are also examined and implications on electrical performance are discussed.

KEYWORDS: carbon nanotubes · Raman spectroscopy · compressive strain · alignment · quartz · nanotube devices

Single-walled carbon nanotubes (SWNTs) possess a combination of exceptional electrical and mechanical properties that may help to advance multiple areas of technology including electronic and electromechanical systems.[1,2] However, as with many nanoscale materials, there remain challenges to overcome before SWNTs can be considered for integration into high performance devices beyond those of proof-of-concept. In general, most applications exploiting unique properties of nanoscale materials will require robust means of patterning/positioning of individual components into ordered assemblies or arrays. Near perfect horizontal alignment on crystalline substrates is arguably the biggest recent advance that has been made toward overcoming this challenge for SWNTs.[3−6] Direct chemical vapor deposition (CVD) of parallel arrays of SWNTs has been achieved on both single crystal quartz and sapphire substrates.[3,5,6] Levels of alignment >99.9% have been demonstrated with growth on quartz.[7] This high degree of alignment is exemplified in Figure 1 where SEM images of two different density samples are shown. For spatially guiding SWNTs perfectly along a particular crystallographic direction at high growth temperatures, relatively strong interaction with the substrate is expected and has been shown to be necessary.[8−10] However, whether or not such an interaction alters the characteristics of the resulting SWNTs has not been considered.

Understanding interactions with the surrounding media including the substrate and controlling them are key challenges to overcome for any nanoscale material en route to applications. However, how the inherent properties of SWNTs are affected by forces that allow horizontal alignment on quartz has not been examined. The local chemical environment and its possible variations can and have led to controversies on our interpretation of observed behavior of SWNTs.[11−20] Elucidating how the interaction with the substrate that enables alignment

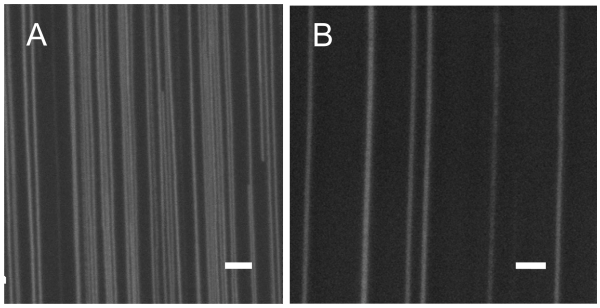

Figure 1. Scanning electron microscope images of aligned SWNTs on single crystal quartz with high (A) and low (B) densities. The scale bars are 2 μm.

*Address correspondence to mshim@illinois.edu.

Received for review May 25, 2009 and accepted July 22, 2009.

Published online July 30, 2009.
10.1021/nn900539t CCC: $40.75

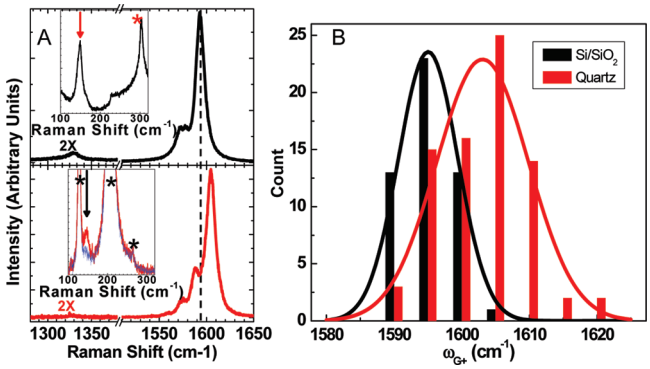

Figure 2. (A) Raman D- and G-band spectra of two different as-grown semiconducting SWNTs on Si/SiO_2 (top, black) and single crystal quartz (bottom, red) substrates. Insets are the corresponding radial breathing mode (RBM) regions. Two SWNTs exhibit nearly identical RBM frequencies indicated by the arrows at148 cm^{-1} for the top spectrum and at 147 cm^{-1} for the bottom spectrum. Peaks indicated by the asterisk (*) are Raman peaks of the substrates. Blue curve in the bottom inset is the Raman spectrum of quartz substrate only. (B) Histograms of G^+ Raman peak frequency distribution of as-grown SWNTs on Si/SiO_2 (black) and single crystal quartz (red) substrates. Histograms are fitted to Gaussians. The average G^+ Raman peak frequency of SWNTs on quartz is up-shifted by ~8 cm^{-1}.

affects desired properties is then critical. Here, we show that the substrate−SWNT interaction leads to nonuniform mechanical strain in aligned SWNTs grown on single crystal quartz. These strained SWNTs in turn allow experimental observation of how difficult-to-achieve uniaxial compression affects vibrational properties of SWNTs. Consequences of device fabrication steps on the nonuniform compressive strain and implications on electrical performance are also discussed.

RESULTS AND DISCUSSION

Compressive Strain Induced G-Band Phonon Frequency Up-Shift and Thermal Response. The Raman spectra of as-grown SWNTs aligned on crystalline quartz often exhibit an anomalous upshift in the G-band phonon mode frequencies. High G-band frequencies have been reported in the very first report of aligned growth on crystalline quartz[3] as well as in Supplementary Figure S3B of ref 21 but have not been explained. The bottom spectrum in Figure 2A demonstrates this anomalous upshift for an as-grown semiconducting SWNT where the G-band longitudinal optical (LO) mode, the G^+ peak, appears at 1605 cm^{-1}. For comparison, the top spectrum is of a typical semiconducting SWNT grown on Si/SiO_2 substrates. For this nonaligned SWNT, the G^+ peak appears at 1593 cm^{-1}. Since metallic SWNTs' Raman spectra are complicated by softening and broadening[22−25] caused by the Kohn anomaly,[24,26,27] our discussion here is limited to semiconducting SWNTs and therefore all acquired G-band spectra have been fitted to Lorentzian peaks.

The insets in Figure 2A show the radial breathing mode (RBM) regions of the two semiconducting SWNTs. The same RBM frequency does not necessarily guarantee that these two are of identical chirality since local variations in the substrate may cause slight shifts in RBM frequencies.[28] However, given nearly identical RBM frequencies, it is possible that these two SWNTs are of the same chirality. More importantly, both theory and experiments indicate that Raman G+ frequency (ω_{G^+}) is independent of diameter and chirality for semiconducting SWNTs.[29,30] Figure 2B compares histograms of ω_{G^+} of 127 isolated semiconducting SWNTs on Si/SiO_2 and on crystalline quartz. From Gaussian fits (solid lines), the average ω_{G^+} for SWNTs aligned on quartz is up-shifted by ~8 cm^{-1}. These observations verify that the anomalous upshift is not a result of chirality-dependent properties but rather a consequence of different interactions with the substrates.

At a fixed temperature and laser energy and intensity, there are three known processes that can affect the G-band Raman spectra of SWNTs: (1) defect introduction,[31,32] (2) doping/carrier injection,[33−35] and, (3) mechanical strain.[36,37] We can minimize potential defect contributions by examining SWNTs with little or no D-band intensities. The histograms in Figure 2B include data only from SWNTs with a D/G intensity ratio <0.05, but including SWNTs with a relatively large D/G ratio does not change the frequency distribution significantly. Most semiconducting SWNTs do not exhibit significant D-band intensities on both types of substrates. When the D-band is observable, the average value and the distribution of D/G ratios are similar for both cases indicating that there is no significant difference in the degree of disorder between SWNTs grown on Si/SiO_2 and single crystalline quartz. Furthermore, in Figure 2, an individual SWNT grown on Si/SiO_2, despite its larger D/G ratio, exhibits ω_{G^+} much closer to the expected phonon frequency than the individual SWNT aligned on quartz, which does not exhibit a detectable D-band intensity. Based on all of these observations, we rule out physical disorder as a possible origin of the anomalous upshift in the G-band frequency.

If we consider the upshift in the G-band frequency to arise solely from doping effects, the degree of doping corresponding to the observed G-band frequency shift may be estimated in the following two ways. First, if we follow Tsang *et al.*[35] and consider phonon energy renormalization due to doping, then the 8 cm^{-1} upshift should correspond to a minimum of ~0.013 (0.004) carriers per C atom for 1 nm (2 nm) diameter semiconducting SWNT. Note that 1 to 2 nm is the diameter range observed for SWNTs grown on both substrates. These are rather high doping levels comparable to those of graphite intercalation compounds and are unlikely to be sufficiently explained by phonon energy renormalization which considers low doping limits. Second, if we then assume that the G-band frequency shift is comparable to that of graphite intercalation compounds following Rao *et al.*,[33] then the 8 cm^{-1} upshift corresponds to an even larger doping fraction difference of 0.017 carriers (holes) per C atom. While the degree of

substrate-induced doping may vary locally,[34] given that quartz and the thermal oxide on Si are both highly insulating, it is unlikely that such a large difference in the average G-band frequency can be accounted for by doping effects. We are then left with the possibility of mechanical strain as the origin of the anomalous upshift in the G-band frequency.

Previous experimental studies have shown that the G-band phonon energy decreases when SWNTs are under uniaxial tension.[38,36,37] Especially with the possibility of electronic structure modification with strain,[39,40] elucidating both tensile and compressive responses of SWNTs is important in terms of fundamental understanding of the material's property as well as enabling new technologies such as nanoelectromechanical systems and flexible electronics. A recent theoretical study has indicated that uniaxial compression of SWNTs should lead to significant up-shifts in the G-band phonon frequencies.[41] However, because of difficulties in applying uniaxial compression, only hydrostatic pressure, often on ensembles of SWNTs, has been experimentally explored.[42−44] Given that relatively strong interaction with the substrate is needed to align along [2$\bar{1}$0] direction at growth temperatures and that the degree of thermal contraction upon cooling should be different for SWNT and crystalline quartz, SWNTs should, in fact, be expected to be under compressive stress. If so, aligned SWNTs on quartz may provide readily accessible experimental conditions to examine often hard-to-achieve uniaxial compression.

To verify that aligned SWNTs grown on single crystal quartz are under compression, we now compare the temperature (T) dependence of Raman G-band frequencies of samples grown on single crystal quartz with that of samples grown on Si/SiO_2. Raman G-band spectra at different T for a typical SWNT grown on Si/SiO_2 and one grown on single crystal quartz are shown in Figure 3, panels A and B, respectively. The near linear T dependence of ω_{G^+} of SWNT on Si/SiO_2 as shown for three different SWNTs in the bottom data set in Figure 3C is expected in the T range studied here and is in quantitative agreement with previous reports.[45−48] From linear curve fits, we obtain the slope for the thermal response of SWNTs on Si/SiO_2 substrate as $(d\omega_{G^+}/dT)_{Si/SiO_2} \approx -0.03$ cm^{-1} K^{-1}. We have observed $(d\omega_{G^+}/dT)_{Si/SiO_2}$ ranging from -0.025 to -0.035 cm^{-1} K^{-1}. Previously reported values range similarly from *ca.* -0.02 to -0.04 cm^{-1} K^{-1}.[45−48] SWNTs grown on single crystal quartz that start out with anomalously upshifted $\omega_{G^+} > 1600$ cm^{-1} at room temperature also exhibit decreasing ω_{G^+} with increasing T as shown in Figure 3B. However, there is a distinct quantitative difference with T response being more than twice as large

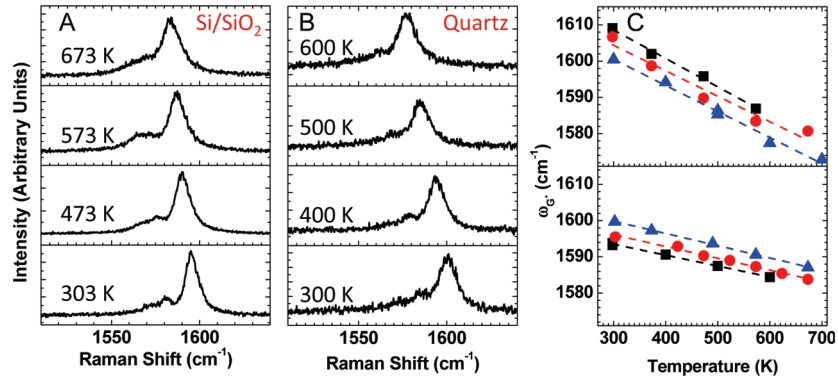

Figure 3. Raman G-band spectra of individual as-grown semiconducting SWNTs on Si/SiO_2 (A) and on single crystal quartz (B) substrates at the indicated temperatures. (C) Temperature dependence of G^+ Raman peak frequencies of several SWNTs grown on quartz (upper graph) and Si/SiO_2 (lower graph) substrates. The dashed lines are linear fits.

$[(d\omega_{G^+}/dT)_{Quartz}$ *ca.* -0.075 cm^{-1} K$^{-1}]$ as shown for three different SWNTs on quartz in the upper graph of Figure 3C. When ω_{G^+} starts out >1600 cm^{-1} at room temperature, we have observed $(d\omega_{G^+}/dT)_{Quartz}$ to vary from -0.07 to -0.08 cm^{-1} K^{-1}, consistently lager than that of SWNTs on Si/SiO_2.

The T response of SWNTs grown on Si/SiO_2 (as well as on quartz when the initial ω_{G^+} is near 1590 cm^{-1}) is similar to the reported results for SWNTs suspended above the substrate (-0.025 cm^{-1} K^{-1} as reported by Zhang *et al.*[48]). They are also very similar to theoretical expectations for graphene E_{2g} mode (G-band) that include 3- and 4-phonon scattering and lattice thermal expansion contributions.[49] Given the similarities between our results for SWNTs on Si/SiO_2 to both theory and experiments including suspended SWNTs, we assume $(d\omega_{G^+}/dT)_{Si/SiO_2}$ *ca.* -0.03 cm^{-1} K^{-1} to be the intrinsic response of semiconducting SWNTs in the absence of mechanical strain. Since the coefficient of thermal expansion (CTE) of Si/SiO_2 and the calculated CTE of SWNTs are similar,[50] it is not surprising that SWNTs on Si/SiO_2 exhibit similar behavior as those suspended above the substrate. Single crystal quartz, on the other hand, exhibits a much larger thermal expansion upon heating. Within the T range studied here, single crystal quartz expands nearly linearly along the SWNT growth direction with CTE $\approx 1.7 \times 10^{-5}$ K^{-1}.[51,52]

Although the axial CTE of SWNTs may depend on chirality, it is expected to be at least about an order of magnitude smaller than that of single crystal quartz along the growth direction.[51−53] Assuming, then, direct thermal expansion of SWNT to be negligible compared to that of the quartz substrate, a change in the uniaxial strain, $d\varepsilon$, of ~0.5% on SWNTs is expected for a T change, dT, of 300 K or $d\varepsilon/dT \approx 0.0017\%$ K^{-1}. For simplicity, if we assume that the substrate induced strain does not alter the inherent anharmonic contributions to T dependent ω_{G^+} shift, we can estimate the mechanical strain component of the observed T dependence as $(d\omega_{G^+}/dT)_{Strain} \approx (d\omega_{G^+}/dT)_{Quartz} - (d\omega_{G^+}/dT)_{Si/SiO_2} = -0.075$ cm^{-1} K^{-1} + 0.03 cm^{-1} K^{-1} = -0.045 cm^{-1} K^{-1}.

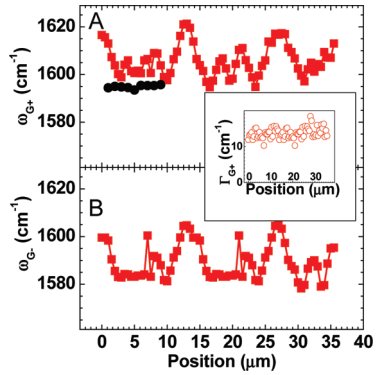

Figure 4. (A) Spatial profile of Raman G^+ peak frequency along the length of an as-grown semiconducting SWNT on a Si/SiO_2 (black circles) and quartz (red squares) substrates. (B) Spatial profile of Raman G^- peak frequency along the length of the same SWNT on quartz (red squares) as in panel A. Inset shows the variation of the line width of the G^+ peak along the aligned SWNT on quartz.

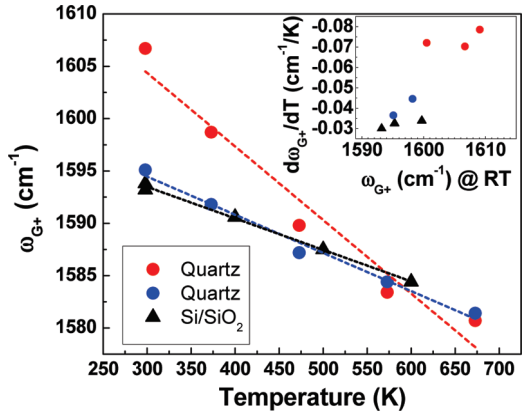

Figure 5. Temperature dependence of Raman G^+ peak frequency of individual SWNTs grown on quartz and on Si/SiO_2. The dashed lines are linear fits. Inset shows the relation between the thermal response of G^+ peak frequency shift and the room-temperature G^+ peak frequency for various SWNTs grown on both types of substrates. In both the inset and the main panel, blues circles correspond to the less frequent regions of low-room-temperature G^+ peak frequency and the red circles correspond to the more common cases of high-room-temperature G^+ peak frequency on quartz. Black triangles are data from SWNTs on Si/SiO_2.

Since the multiphonon terms are expected to dominate over the lattice expansion contribution in the inherent T dependence of ω_{G^+},[45,47−50] this is a reasonable assumption. We then have $d\omega_{G^+}/d\varepsilon \approx -27$ cm^{-1}/% strain in excellent agreement with calculated value of *ca.* −24 cm^{-1}/% strain for a semiconducting (17, 0) SWNT in the small strain limit.[41] These results, combined with the fact that compressive stress leads to an upshift in ω_{G^+} whereas tensile stress leads to a downshift, indicate that horizontally aligned SWNTs grown on single crystal quartz substrate are, on average, under significant axial compression. The range of observed upshift in ω_{G^+} corresponds to a maximum compressive strain of up to ∼1.1% (assuming zero-strain ω_{G^+} to be 1590 cm^{-1}). This is already a substantial amount, but we suspect that there may be local regions of even higher degree of strain as discussed in the next section.

Non-Uniformity of Axial Strain and its Origin. Having established that the observed anomalous average ω_{G^+} upshift and the large T response arise from single crystal quartz substrates inducing uniaxial compression, we now examine ω_{G^+} along the length of individual SWNTs. Figure 4 compares ω_{G^+} along a SWNT grown on Si/SiO_2 with that of one grown on quartz. As expected, there is very little variation (<1 cm^{-1}) on SWNT grown on Si/SiO_2 substrate as shown in Figure 4A. However, large and apparently random fluctuations (standard deviation of ∼7 cm^{-1}) in ω_{G^+} of SWNTs aligned on single crystal quartz are evident. The G^- peak frequency (ω_{G^-}) variations along the length of the same SWNT, shown in Figure 4B, follow ω_{G^+} fluctuations closely. The line width (Γ_{G^+}), on the other hand, appears to be independent of the G-band peak frequency variations (Figure 4 inset). While there is no obvious periodicity or trend, these ω_{G^+} fluctuations with the minimum value always being greater than 1590 cm^{-1} suggest nonuniform compressive strain along the length of SWNTs.

To verify the nonuniformity of the substrate-induced compressive strain, we again examine how ω_{G^+} varies with T. Figure 5 shows the T dependence of ω_{G^+} at two different locations of the same SWNT. Red circles are from a location with anomalously up-shifted ω_{G^+} at room temperature (1607 cm^{-1}), and the blue circles are from a nearby location with "normal" (or unstrained) ω_{G^+} at room temperature (1595 cm^{-1}). Results from a SWNT grown on Si/SiO_2 are also shown for comparison. The anomalous initial ω_{G^+} region has a large $d\omega_{G^+}/dT \approx -0.07$ cm^{-1} K^{-1}, whereas the "normal" initial ω_{G^+} region follows the same trend as SWNTs on Si/SiO_2. That is, only regions with initial high ω_{G^+} values are under compressive strain. The inset shows the near linear dependence of thermal response of ω_{G^+} shift on the initial room temperature ω_{G^+} values for SWNTs on both Si/SiO_2 and quartz substrates. The spatial variations both in ω_{G^+} and $d\omega_{G^+}/dT$ support the idea that the compressive strain in as-grown SWNTs on quartz is nonuniform in nature.

Given the necessity of strong interaction for alignment and the large difference in CTE with the substrate, the presence of significant compressive strain in SWNTs aligned on quartz is, at least in hindsight, not surprising. However, the nonuniformity may be somewhat unexpected. To address the origin of this nonuniformity, we now consider surface roughness of the substrate. Figure 6 compares Raman G-band image with the corresponding AFM image of two adjacent aligned SWNTs on single crystal quartz. One of the gold markers deposited prior to CVD growth to ensure that the same location is being studied is also visible on the right edge of both images. Figure 6B is the G-band intensity map where we have integrated area only between 1590

and 1600 cm^{-1}. This selective Raman map highlights parts of SWNTs where there is minimal strain (*i.e.*, regions where ω_{G^+} values are close to the "normal" expected frequency of ~1590 to 1595 cm^{-1} correspond to the bright spots). Figure 6A is a composite of 2 AFM images where the middle part has been collected at a higher resolution and has been adjusted to highlight the surface roughness of the single crystal quartz substrate. The parallel lines that are at ~30° to the SWNT alignment direction are presumably polishing scratches—the vendor has indicated that the substrates have been polished with cerium oxide slurry with a polyurethane pad. While the polishing scratches are mostly parallel with each other and unidirectional at this magnification; their density, depth, and width appear to vary randomly. Comparison between the Raman G-band map and the AFM image reveals a striking correlation in the direction of the polishing scratch lines with the alignment of locations of ω_{G^+} minima in the two neighboring SWNTs as indicated by the double-headed arrows. That is, the alignment of regions of minimum strain in the neighboring SWNTs coincides with the direction of polishing induced roughness. On the basis of this observation, we propose that the nonuniformity of compressive strain along the SWNT arises from variations in the interaction with the substrate due to the surface roughness caused mainly by polishing scratches. The random variations in ω_{G^+} and in $d\omega_{G^+}/dT$ along the length of a SWNT are then likely to be arising from the distributions of density, depth, and width of these scratches. While the strong interaction with the substrate and the large difference in CTE lead to compressive strain, these scratches create small "trenches" underneath the SWNTs that provide regions free of or at least reduced degree of strain.

We note that the widths of the polishing scratches are much smaller than our laser spot size of ~1 μm. Therefore, each Raman spectrum obtained here actually provides an average ω_{G^+} value that reflects the density of these scratch lines on the substrate. That is, within the laser spot, some parts of the SWNT will be over the polishing scratches while other parts will not. This then implies that there are local regions where the compressive strain may be significantly larger than the maximum ~1% that we have estimated based on the maximum ω_{G^+} observed at room temperature.

Effects of Device Fabrication on the Nonuniform Strain. Previous studies have shown that the electronic band gaps of SWNTs can be altered by mechanical stress.[40] The substrate-induced nonuniform uniaxial compression on as-grown SWNTs horizontally aligned on single crystal quartz may then affect electrical characteristics of SWNT-based devices. On the contrary, transistors consisting of SWNTs grown on quartz exhibit performances comparable to those of SWNTs on Si/SiO_2 substrates. For example, the inferred average per tube mobility of devices made of parallel arrays of thousands of SWNTs

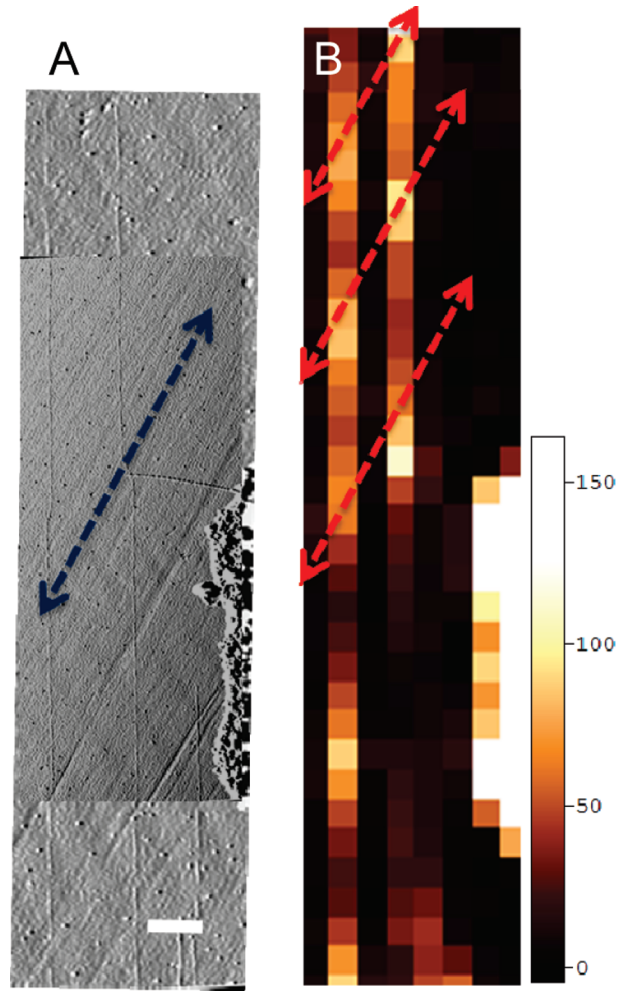

Figure 6. Side-by-side comparison of a composite AFM image (A) with Raman intensity map integrated between 1590 and 1600 cm^{-1} and (B) of the same area showing SWNTs on single crystal quartz at room temperature. Scale bar of the AFM image corresponds to 1 μm. Raman map is at the same magnification. Intensity scale bar for the Raman map is shown on the right of panel B. The blue arrow in panel A indicates the direction of the polishing scratches. Three red arrows in panel B point in the same direction as the arrow in panel A and are placed over the bright spots in the Raman image indicating the alignment direction of low-strain points being coincidental with the polishing scratches.

on quartz has been shown to be similar to the mobility of individual SWNTs on Si/SiO_2 substrates.[4] The sign and the magnitude of the change in the band gap due to strain depend on the chiral angle.[40,54] Roughly the same percentage of SWNTs will have widening of the gap as those that have gap closing. The magnitudes of changes in the band gaps are also expected to be relatively small—most are within ~100 meV range for 2% uniaxial strain.[54] Therefore, the net effect of compressive strain due to the substrate in devices consisting of large numbers of SWNTs in parallel arrays is expected to be negligible at room temperature. In individual SWNT devices, on the other hand, there may be significant differences for certain chiralities. While it is difficult to quantify differences in the electrical properties of individual SWNT transistors fabricated on quartz *vs* on Si/

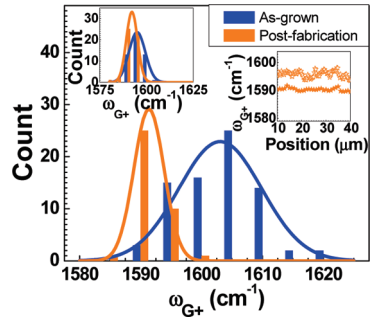

Figure 7. Distribution of Raman G$^+$ peak frequencies of as-grown SWNTs on single crystal quartz substrates before (blue) and after (orange) device fabrication. The upper left inset displays the same comparison for SWNTs on Si/SiO$_2$ substrates. The right inset shows the spatial profile of Raman G+ frequency along the length of two different SWNTs on quartz substrates after device fabrication.

SiO_2 substrates due to large device-to-device variations (*e.g.*, contact resistance variations, different degree of disorder, *etc.*), our Raman studies suggest that such differences should not even be expected. Figure 7 shows that the average ω_{G^+} down-shifts from 1603 to 1591 cm^{-1} upon photolithography and metallization. The right inset in Figure 7 shows ω_{G^+} along the length of two different semiconducting SWNTs after device fabrication steps. While some of the fluctuations in ω_{G^+} remain, the standard deviations are less than 1.5 cm^{-1} and the actual ω_{G^+} vales are now much closer to the expected range of 1590−1595 cm^{-1} for unstrained semiconducting SWNTs. These results indicate that most of the compressive strain due to the quartz substrate is relieved during device fabrication steps.

Finally, we note that the average ω_{G^+} of SWNTs on Si/SiO_2 substrates also down-shifts after device fabrication steps. Upper left inset of Figure 7 shows that SWNTs grown on Si/SiO_2 substrates also exhibit a down-shift from 1595 to 1592 cm^{-1} upon lithography and metallization. While the magnitude of this down-shift is smaller, it may not be negligible. We suspect that a combination of changes in doping level and in defects may be responsible for the down-shift in these unstrained SWNTs.

CONCLUSIONS

We have shown that, on average, as-grown SWNTs horizontally aligned on single crystal quartz exhibit anomalously up-shifted G-band phonon energies. The magnitude of the upshift can be as large as ~30 cm^{-1} and it is nonuniform along the length of SWNTs. The nonuniformity arises from the surface roughness of the polishing scratches. Comparison of *T* dependences of ω_{G^+} of SWNTs grown on quartz and on Si/SiO_2 substrates has revealed that these unusual phonon frequencies are the consequences of mechanical compression induced by the substrate. Strong interactions with the substrate that allows nearly perfect alignment when combined with a large difference in CTE leave the SWNTs under nonuniform but uniaxial compressive strain at room temperature. These strained SWNTs in turn allow effects of difficult-to-achieve uniaxial compressive stress to be experimentally examined. Our results open up the possibility of comparing metallic *vs* semiconducting SWNTs' responses and verification of chirality dependent responses to uniaxial compressive stress. We have also shown that typical device fabrication steps relieve the compressive strain in horizontally aligned SWNTs and the resulting electrical characteristics are expected and are observed to be similar to SWNTs grown on Si/SiO_2 substrates.

METHODS

SWNTs were grown by CVD on both preannealed ST-cut single crystal quartz[7] (Hoffman Materials) and Si/SiO_2 (300 nm thermal oxide). Ferritin or e-beam evaporated Fe patterns and EtOH vapor were used as catalyst and the carbon source, respectively, following previous reports.[3,7] To check for possible variations from growth to growth affecting the results, samples on quartz and Si/SiO_2 substrates grown in the same furnace simultaneously were also compared, but the results were the same as comparison across samples grown at different times. Only samples with low density (<1 SWNT/μm) were used to ensure that the results were not complicated by Raman signals from multiple SWNTs. Raman spectra were collected using a Jobin−Yvon confocal Raman microscope through a 100× air objective with a 633 nm laser source. The laser spot size was ~1 μm and the laser power was kept at 4.5 mW. The backscattered light was collected through a confocal hole and 1800 grooves/mm grating to a thermoelectrically cooled CCD detector with each pixel representing ~0.3 cm^{-1}. Unless otherwise noted, all spectra were collected on as-grown SWNTs where the last step before data collection was the CVD growth. For temperature-dependence measurements, SWNTs were heated under Ar flow in a controlled environment chamber with an optical window for Raman measurements.[55] To examine the effects of device fabrication steps, two terminal Ti/Au electrodes were deposited on as-grown SWNTs on both quartz and Si/SiO_2 substrates by electron beam evaporation after patterning *via* photolithography (Shipley 1805 and PMMA resists) or e-beam lithography (PMMA).[56,57]

Acknowledgment. We thank C. Kocabas and S. MacLaren for helpful discussions. This material is based upon work supported by the NSF (Grants No. CCF-0506660 and No. DMR-0348585). Scanning electron microscopy and atomic force microscopy were carried out in the Center for Microanalysis of Materials, University of Illinois at Urbana−Champaign, which is partially supported by the U.S. Department of Energy under Grant No. DEFG02-91-ER45439.

REFERENCES AND NOTES

1. Saito, R.; Dresselhaus, G.; Dresselhaus, M. S. *Physical Properties of Carbon Nanotubes*; Imperial College Press: London, 1998; pp 208−209.
2. Baughman, R. H.; Zakhidov, A. A.; de Heer, W. A. Carbon Nanotubes—The Route Toward Applications. *Science* **2002**, *297*, 787–792.
3. Kocabas, C.; Hur, S. H.; Gaur, A.; Meitl, M. A.; Shim, M.; Rogers, J. A. Guided Growth of Large-Scale, Horizontally Aligned Arrays of Single-Walled Carbon Nanotubes and Their Use in Thin-Film Transistors. *Small* **2005**, *1*, 1110–1116.

4. Kang, S. J.; Kocabas, C.; Ozel, T.; Shim, M.; Pimparkar, N.; Alam, M. A.; Rotkin, S. V.; Rogers, J. A. High-Performance Electronics Using Dense, Perfectly Aligned Arrays of Single-Walled Carbon Nanotubes. *Nat. Nanotechnol.* **2007**, *2*, 230–236.
5. Han, S.; Liu, X.; Zhou, C. Template-Free Directional Growth of Single-Walled Carbon Nanotubes on a- and r-Plane Sapphire. *J. Am. Chem. Soc.* **2005**, *127*, 5294–5295.
6. Ismach, A.; Segev, L.; Wachtel, E.; Joselevich, E. Atomic-Step-Templated Formation of Single Wall Carbon Nanotube Patterns. *Angew. Chem., Int. Ed.* **2004**, *43*, 6140–6143.
7. Kocabas, C.; Kang, S. J.; Ozel, T.; Shim, M.; Rogers, J. A. Improved Synthesis of Aligned Arrays of Single-Walled Carbon Nanotubes and their Implementation in Thin Film Type Transistors. *J. Phys. Chem. C* **2007**, *111*, 17879–17886.
8. Ishigami, N.; Ago, H.; Imamoto, K.; Tsuji, M.; Iakoubovskii, K.; Minami, N. Crystal Plane Dependent Growth of Aligned Single-Walled Carbon Nanotubes on Sapphire. *J. Am. Chem. Soc.* **2008**, *130*, 9918–9924.
9. Yu, Q.; Qin, G.; Li, H.; Xia, Z.; Nian, Y.; Pei, S. S. Mechanism of Horizontally Aligned Growth of Single-Wall Carbon Nanotubes on R-Plane Sapphire. *J. Phys. Chem. B* **2006**, *110*, 22676–22680.
10. Liu, X.; Ryu, K.; Badmaev, A.; Han, S.; Zhou, C. Diameter Dependence of Aligned Growth of Carbon Nanotubes on a-Plane Sapphire Substrates. *J. Phys. Chem. C* **2008**, *112*, 15929–15933.
11. Chen, R. J.; Franklin, N. R.; Kong, J.; Cao, J.; Tombler, T. W.; Zhang, Y.; Dai, H. Molecular Photodesorption from Single-Walled Carbon Nanotubes. *Appl. Phys. Lett.* **2001**, *79*, 2258–2260.
12. Collins, P. G.; Bradley, K.; Ishigami, M.; Zettl, A. Extreme Oxygen Sensitivity of Electronic Properties of Carbon Nanotubes. *Science* **2000**, *287*, 1801–1804.
13. Dukovic, G.; White, B. E.; Zhou, Z.; Wang, F.; Jockusch, S.; Steigerwald, M. L.; Heinz, T. F.; Friesner, R. A.; Turro, N. J.; Brus, L. E. Reversible Surface Oxidation and Efficient Luminescence Quenching in Semiconductor Single-Wall Carbon Nanotubes. *J. Am. Chem. Soc.* **2004**, *126*, 15269–15276.
14. Heinze, S.; Tersoff, J.; Martel, R.; Derycke, V.; Appenzeller, J.; Avouris, P. Carbon Nanotubes as Schottky Barrier Transistors. *Phys. Rev. Lett.* **2002**, *89*, 106801–106804.
15. Jhi, S.; Louie, S. G.; Cohen, M. L. Electronic Properties of Oxidized Carbon Nanotubes. *Phys. Rev. Lett.* **2000**, *85*, 1710–1713.
16. Shim, M.; Back, J. H.; Ozel, T.; Kwon, K. W. Effects of Oxygen on the Electron Transport Properties of Carbon Nanotubes: Ultraviolet Desorption and Thermally Induced Processes. *Phys. Rev. B* **2005**, *71*, 205411.
17. Shim, M.; Siddons, G. P. Photoinduced Conductivity Changes in Carbon Nanotube Transistors. *Appl. Phys. Lett.* **2003**, *83*, 3564–3566.
18. Sumanasekera, G. U.; Adu, C. K. W.; Fang, S.; Eklund, P. C. Effects of Gas Adsorption and Collisions on Electrical Transport in Single-Walled Carbon Nanotubes. *Phys. Rev. Lett.* **2000**, *85*, 1096–1099.
19. Ulbricht, H.; Moos, G.; Hertel, T. Interaction of Molecular Oxygen with Single-Wall Carbon Nanotube Bundles and Graphite. *Surf. Sci.* **2003**, *532−535*, 852–856.
20. Shim, M.; Gaur, A.; Nguyen, K. T.; Abdula, D.; Ozel, T. Spectral Diversity in Raman G-Band Modes of Metallic Carbon Nanotubes within a Single Chirality. *J. Phys. Chem. C* **2008**, *112*, 13017–13023.
21. Ding, L.; Tselev, A.; Wang, J.; Yuan, D.; Chu, H.; McNicholas, T. P.; Li, Y.; Liu, J. Selective Growth of Well-Aligned Semiconducting Single-Walled Carbon Nanotubes. *Nano Lett.* **2009**, *9*, 800–805.
22. Nguyen, K. T.; Gaur, A.; Shim, M. Fano Lineshape and Phonon Softening in Single Isolated Metallic Carbon Nanotubes. *Phys. Rev. Lett.* **2007**, *98*, 145504.
23. Wu, Y.; Maultzsch, J.; Knoesel, E.; Chandra, B.; Huang, M.; Sfeir, M. Y.; Brus, L. E.; Hone, J.; Heinz, T. F. Variable Electron-Phonon Coupling in Isolated Metallic Carbon Nanotubes Observed by Raman Scattering. *Phys. Rev. Lett.* **2007**, *99*, 027402.
24. Ando, T. Anomaly of Optical Phonon in Monolayer Graphene. *J. Am. Chem. Soc.* **2006**, *75*, 124701.
25. Farhat, H.; Son, H.; Samsonidze, G. G.; Reich, S.; Dresselhaus, M. S.; Kong, J. Phonon Softening in Individual Metallic Carbon Nanotubes Due to the Kohn Anomaly. *Phys. Rev. Lett.* **2007**, *99*, 145506.
26. Caudal, N.; Saitta, A. M.; Lazzeri, M.; Mauri, F. Kohn Anomalies and Nonadiabaticity in Doped Carbon Nanotubes. *Phys. Rev. B* **2007**, *75*, 115423.
27. Piscanec, S.; Lazzeri, M.; Mauri, F.; Ferrari, A. C.; Robertson, J. Kohn Anomalies and Electron-Phonon Interactions in Graphite. *Phys. Rev. Lett.* **2004**, *93*, 185503.
28. Zhang, Y.; Zhang, J.; Son, H.; Kong, J.; Liu, Z. Substrate-Induced Raman Frequency Variation for Single-Walled Carbon Nanotubes. *J. Am. Chem. Soc.* **2005**, *127*, 17156–17157.
29. Jorio, A.; Souza Filho, A. G.; Dresselhaus, G.; Dresselhaus, M. S.; Swan, A. K.; Unlu, M. S.; Goldberg, B. B.; Pimenta, M. A.; Hafner, J. H.; Lieber, C. M.; Saito, R. G-Band Resonant Raman Study of 62 Isolated Single-Wall Carbon Nanotubes. *Phys. Rev. B* **2002**, *65*, 155412.
30. Dubay, O.; Kresse, G.; Kuzmany, H. Phonon Softening in Metallic Nanotubes by a Peierls-Like Mechanism. *Phys. Rev. Lett.* **2002**, *88*, 235506.
31. Wang, C. J.; Cao, Q.; Ozel, T.; Gaur, A.; Rogers, J. A.; Shim, M. Electronically Selective Chemical Functionalization of Carbon Nanotubes: Correlation between Raman Spectral and Electrical Responses. *J. Am. Chem. Soc.* **2005**, *127*, 11460–11468.
32. Nguyen, K. T.; Shim, M. Role of Covalent Defects on Phonon Softening in Metallic Carbon Nanotubes. *J. Am. Chem. Soc.* **2009**, *131*, 7103–7106.
33. Rao, A. M.; Eklund, P. C.; Bandow, S.; Thess, A.; Smalley, R. E. Evidence for Charge Transfer in Doped Carbon Nanotube Bundles from Raman Scattering. *Nature* **1997**, *388*, 257–259.
34. Shim, M.; Ozel, T.; Gaur, A.; Wang, C. J. Insights on Charge Transfer Doping and Intrinsic Phonon Line Shape of Carbon Nanotubes by Simple Polymer Adsorption. *J. Am. Chem. Soc.* **2006**, *128*, 7522–7530.
35. Tsang, J. C.; Freitag, M.; Perebeinos, V.; Liu, J.; Avouris, P. Doping and Phonon Renormalization in Carbon Nanotubes. *Nat. Nanotechnol.* **2007**, *2*, 725–730.
36. Cronin, S. B.; Swan, A. K.; Unlu, M. S.; Goldberg, B. B.; Dresselhaus, M. S.; Tinkham, M. Measuring the Uniaxial Strain of Individual Single-Wall Carbon Nanotubes: Resonance Raman Spectra of Atomic-Force-Microscope Modified Single-Wall Nanotubes. *Phys. Rev. Lett.* **2004**, *93*, 167401.
37. Cronin, S. B.; Swan, A. K.; Unlu, M. S.; Goldberg, B. B.; Dresselhaus, M. S.; Tinkham, M. Resonant Raman Spectroscopy of Individual Metallic and Semiconducting Single-Wall Carbon Nanotubes Under Uniaxial Strain. *Phys. Rev. B* **2005**, *72*, 035425.
38. Gao, B.; Jiang, L.; Ling, X.; Zhang, J.; Liu, Z. F. Chirality-Dependent Raman Frequency Variation of Single-Walled Carbon Nanotubes Under Uniaxial Strain. *J. Phys. Chem. C* **2008**, *112*, 20123–20125.
39. Tombler, T. W.; Zhou, C.; Alexseyev, L.; Kong, J.; Dai, H.; Liu, L.; Jayanthi, C. S.; Tang, M.; Wu, S. Y. Reversible Electromechanical Characteristics of Carbon Nanotubes Under Local-Probe Manipulation. *Nature* **2000**, *405*, 769–772.
40. Minot, E. D.; Yaish, Y.; Sazonova, V.; Park, J. Y.; Brink, M.; McEuen, P. L. Tuning Carbon Nanotube Band Gaps with Strain. *Phys. Rev. Lett.* **2003**, *90*, 156401.
41. Yang, W.; Wang, R.; Yan, H. Strain-Induced Raman-Mode Shift in Single-Wall Carbon Nanotubes: Calculation of Force Constants from Molecular-Dynamics Simulations. *Phys. Rev. B* **2008**, *77*, 195440.
42. Amer, M. S.; El-Ashry, M. M.; Maguire, J. F. Study of the Hydrostatic Pressure Dependence of the Raman Spectrum

of Single-Walled Carbon Nanotubes and Nanospheres. *J. Chem. Phys.* **2004**, *121*, 2752–2757.
43. Venkateswaran, U. D.; Rao, A. M.; Richter, E.; Menon, M.; Rinzler, A.; Smalley, R. E.; Eklund, P. C. Probing the Single-Wall Carbon Nanotube Bundle: Raman Scattering under High Pressure. *Phys. Rev. B* **1999**, *59*, 10928–10934.
44. Lebedkin, S.; Arnold, K.; Kiowski, O.; Hennrich, F.; Kappes, M. M. Raman Study of Individually Dispersed Single-Walled Carbon Nanotubes Under Pressure. *Phys. Rev. B* **2006**, *73*, 094109.
45. Li, H. D.; Yue, K. T.; Lian, Z. L.; Zhan, Y.; Zhou, L. X.; Zhang, S. L.; Shi, Z. J.; Gu, Z. N.; Liu, B. B.; Yang, R. S.; Yang, H. B.; Zou, G. T.; Zhang, Y.; Iijima, S. Temperature Dependence of the Raman Spectra of Single-Wall Carbon Nanotubes. *Appl. Phys. Lett.* **2000**, *76*, 2053–2055.
46. Chiashi, S.; Murakam, Y.; Miyauchi, Y.; Maruyama, S. Temperature Dependence of Raman Scattering from Single-Walled Carbon Nanotubes: Undefined Radial Breathing Mode Peaks at High Temperatures. *Jpn. J. Appl. Phys.* **2008**, *47*, 2010–2015.
47. Zhang, Q.; Yang, D. J.; Wang, S. G.; Yoon, S. F.; Ahn, J. Influences of Temperature on the Raman Spectra of Single-Walled Carbon Nanotubes. *Smart Mater. Struct.* **2006**, *15*, S1–S4.
48. Zhang, Y. Y.; Xie, L. M.; Zhang, J.; Wu, Z. Y.; Liu, Z. F. Temperature Coefficients of Raman Frequency of Individual Single-Walled Carbon Nanotubes. *J. Phys. Chem. C* **2007**, *111*, 14031–14034.
49. Bonini, N.; Lazzeri, M.; Marzari, N.; Mauri, F. Phonon Anharmonicities in Graphite and Graphene. *Phys. Rev. Lett.* **2007**, *99*, 176802.
50. Raravikar, N. R.; Keblinski, P.; Rao, A. M.; Dresselhaus, M. S.; Schadler, L. S.; Ajayan, P. M. Temperature Dependence of Radial Breathing Mode Raman Frequency of Single-Walled Carbon Nanotubes. *Phys. Rev. B* **2002**, *66*, 235424.
51. Jay, A. H. The Thermal Expansion of Quartz by X-Ray Measurements. *Proc. R. Soc. London, A* **1933**, *142*, 237–247.
52. Rosenholtz, J. L.; Smith, D. T. Linear Thermal Expansion and Inversions of Quartz, Var. Rock Crystal. *Am. Mineral.* **1941**, *26*, 103.
53. Jiang, H.; Liu, B.; Huang, Y.; Hwang, K. C. Thermal Expansion of Single Wall Carbon Nanotubes. *J. Eng. Mater. Technol.* **2004**, *126*, 265–270.
54. Huang, M. Y.; Wu, Y.; Chandra, B.; Yan, H.; Shan, Y.; Heinz, T. F.; Hone, J. Direct Measurement of Strain-Induced Changes in the Band Structure of Carbon Nanotubes. *Phys. Rev. Lett.* **2008**, *100*, 136803.
55. Gaur, A.; Shim, M. Substrate-Enhanced O-2 Adsorption and Complexity in the Raman G-Band Spectra of Individual Metallic Carbon Nanotubes. *Phys. Rev. B* **2008**, *78*, 125422.
56. Ozel, T.; Gaur, A.; Rogers, J. A.; Shim, M. Polymer Electrolyte Gating of Carbon Nanotube Network Transistors. *Nano Lett.* **2005**, *5*, 905–911.
57. Kocabas, C.; Dunham, S.; Cao, Q.; Cimino, K.; Ho, X.; Kim, H. S.; Dawson, D.; Payne, J.; Stuenkel, M.; Zhang, H.; Banks, T.; Feng, M.; Rotkin, S. V.; Rogers, J. A. High-Frequency Performance of Submicrometer Transistors That Use Aligned Arrays of Single-Walled Carbon Nanotubes. *Nano Lett* **2009**, *9*, 1937–1943.